

# A boundary element approach to ocean seismoacoustic facet reverberation

Peter Gerstoft

*Ødegaard and Danneskiold-Samsøe, Kroghsgade 1, 2100 Copenhagen, Denmark and Massachusetts Institute of Technology, Cambridge, Massachusetts 02139*

Henrik Schmidt

*Massachusetts Institute of Technology, Cambridge, Massachusetts 02139*

(Received 27 July 1990; accepted for publication 29 October 1990)

A numerically efficient, hybrid method is introduced for modeling of short and long range seismoacoustic facet reverberation in the ocean environment. The method combines the global matrix approach to the solution of the wave equation in horizontally stratified media with a boundary element formulation of the boundary conditions at a contour surrounding the facet. The present paper describes a two-dimensional formulation for facets within an elastic seabed or an elastic ice cover, but allows for simulation of the reverberant field within the water column as well. The approach is directly extendable to treat reverberation from seabed-penetrating facets as well as three-dimensional elastic facets. In contrast to discrete methods such as the finite element and finite difference approaches, the solution obtained with the present hybrid approach is not only efficient for short- as well as long-range reverberation, but inherently decomposes the total solution in the temporal and spatial spectral components, of importance to the basic physical understanding of the factors affecting seismoacoustic facet reverberation.

PACS numbers: 43.30.Gv, 43.30.Bp, 43.30.Ma

## INTRODUCTION

The effect of noise correlation on the performance of ocean acoustic array processing is well established, making it important to include such effects in theoretical evaluations of signal processing algorithms.<sup>1</sup> The effect of the noise is obviously more severe the more "signal-like" the noise is. Thus the "white" electronic noise is less of a problem than surface generated noise<sup>2</sup> or shipping noise.

Another correlated noise component is that generated by the signal itself through scattering and reverberation. However, in contrast to the, e.g., surface generated ambient noise, the reverberant field is directly associated with and dependent on the signal to be extracted by the signal processing. Therefore, the reverberant field will both be proportional to the signal strength and often have spatial correlation characteristics that are more "signal-like" than those of the ambient noise, in turn providing more problems for the signal processing performance.

The degradation of the signal processing performance is closely related to the degree and nature of the correlation. To enable performance analysis of signal processing algorithms, it is therefore essential to be able to accurately model the array response to scattering and reverberation in realistic ocean environments.

Based on the temporal and spatial correlation characteristics, the reverberation is divided into two main categories, *diffuse* and *facet* reverberation. The *diffuse* reverberation is due to scattering by the small-scale, stochastic structure of the ocean waveguide, e.g., surface and bottom roughness, and bottom inhomogeneity. The *facet* reverbera-

tion is due to abrupt changes in the environment, e.g., by seamounts and subbottom faults and diapirs. Due to its stochastic nature, the *diffuse* reverberation is characterized by a relatively low correlation. The ocean facets are of more deterministic nature and therefore give rise to extremely "signal-like" reverberation.

Due to theoretical and computational limitations, the numerical modeling tools applied in underwater acoustics have until recently been limited to one-way, two-dimensional propagation scenarios, capable of treating the reverberation problem only in terms of "target strength," incapable of representing real ocean reverberation. Thus available theories cannot explain the reverberation received from the continental margins as well as the reverberant field observed in apparently smooth ocean environments.

On this background there has been a significant effort in recent years to improve the modeling capabilities to incorporate scattering and reverberation effects.

Most theoretical work on *diffuse* scattering has been focusing on the rough sea surface, where various scattering theories have been developed. A very thorough review of these approaches was recently given by Thorsos and Jackson.<sup>3</sup> The elastic properties of the ocean bottom become important at low frequencies in particular, but not until very recently have elastic effects been incorporated in the theoretical analysis of rough bottom scattering.<sup>4,5</sup> A review of earlier work on bottom scattering is given by Ogilvy.<sup>6</sup>

The *facet* reverberation is due to local, distinct features in the environment. The coupled mode approach of Evans<sup>7</sup> is capable of modeling the reverberation from two-dimen-

sional facets, but is limited to purely fluid environments. It is therefore inapplicable to analysis of elastic scattering by ice and bottom facets. For such problems, discrete methods such as the finite difference (FD) approach has been applied to bottom scattering<sup>8</sup> and arctic ice keel scattering.<sup>9</sup> The discrete methods are very general in terms of geometries that can be treated, but the computational requirements are substantial due to the fact that the entire environment has to be discretized with a grid size small compared to the wavelengths involved. These methods are therefore for all practical purposes limited to short-range two-dimensional reverberation problems. For the same reason, extension to three dimensions is prohibitive, although possible in principle. Other problems for the discrete methods are the radiation condition at the boundary of the computational mesh as well as numerical dispersion introduced by the discretization.

Some of the most developed approaches for ocean acoustic and seismic propagation are the wavenumber integration (WI) methods based on separation of variables through integral transforms, both for time and frequency domain analysis.<sup>10-13</sup> One of the main advantages of the integral transform methods is the inherent decomposition of the total solution in both temporal and spatial spectral components, enabling interpretation of the results in terms of basic wave physics. The disadvantage of the integral transform methods are their geometric inflexibility, limiting their direct applicability to problems with separable geometry, e.g., a horizontally stratified ocean.

However, the wave number integration methods can be applied to the facet reverberation problem in a hybrid scheme. Thus Ingenito<sup>14</sup> and Hackman *et al.*<sup>15</sup> use a *T*-matrix approach to represent the scattered field that is then convolved with the waveguide Green's function to produce the waveguide reverberation. In their approach multiple scattering is accounted for through a scattering series.

The same problem can be solved in a self-consistent manner using Green's theorem for the surface of this facet, requiring a finite discretization of the surface for numerical implementation. The boundary element method (BEM) combines an integral representation of the wave field within a volume with a point representation of stresses and displacements on the boundary between the two domains. The need for a dense mesh is limited to this boundary alone, eliminating the problem of discretely representing the wave field throughout the volume. This feature makes the BEM approach advantageous to scattering and radiation problems.

Several boundary element formulations based on wave number integration for the Green's functions have been presented. However, they have all been formulated for either purely fluid or purely elastic media, none of which is directly applicable to the ocean seismoacoustic reverberation problem. Schuster and Smith<sup>16</sup> combined a boundary integral method with a wave number integration approach to analyze scattering by rigid inclusions in a stratified fluid waveguide. Dawson and Fawcett<sup>17</sup> used a similar approach to address the reverberation from the waveguide boundaries. However, both were limited to fluid waveguides and ideal, homogeneous boundary conditions.

There has been a significant effort in the seismic community in applying the hybrid BEM-WI approach to elastic scattering problems. Bravo *et al.*<sup>18</sup> investigated the ground motion for *SH* waves due to a layered alluvial valley in an elastic half-space and Campillo<sup>19</sup> modeled the reverberation of *SH* waves from a salt dome, where both interior and exterior domains were considered a layered media. The more complex *P-SV* problem has been addressed by Bouchon and Aki.<sup>11</sup> By assuming periodicity in the horizontal, they discretized all boundaries in the stratification and use wave number integration to determine the free-field Green's functions, with the discretization determined from the spatial sampling theorem. Thus the discretization is equidistant in the horizontal, making the approach inapplicable to, e.g., facets with vertical boundaries as pointed out by Bouchon.<sup>20</sup> This problem has been solved for elastic half-space problems by Kawase.<sup>21</sup> He interchanged the element and wave number integrations, allowing the element integral to be evaluated in closed form for each wave number component, assuming constant displacement and stress along each element. This approach has been applied to several seismic problems by Kawase and Aki.<sup>22,23</sup>

In the present paper we generalize the approach of Kawase<sup>21</sup> to incorporate linear variation of the field parameters over the elements. Further, we will formulate the boundary element representation such that both the exterior and interior domains may be stratified with any combination of acoustic, elastic, and transversely isotropic layers. This is achieved by integrating the boundary element method with the direct global matrix approach<sup>12,24</sup> to propagation in stratified ocean environments.

We will here limit the analysis to two-dimensional facets that are entirely enclosed in elastic media, thus allowing for simulation of reverberation from subbottom facets such as salt diapirs and ice facets such as grooves. In a subsequent paper, we will extend the formulation to allow analysis of reverberation from facets in contact with both elastic and fluid layers, such as seamounts and ice keels.

The paper first outlines the problem under consideration. Then the boundary integral representation of an elastic wave field is described, followed by the boundary element formulation. The global matrix approach to the solution of the depth separated wave equation is briefly summarized in the context of the present boundary element formulation, including the closed form integration of the boundary element contributions. The numerical examples examine the reverberation from a groove in an arctic ice cover and an elastic subbottom facet.

## I. STATEMENT OF PROBLEM

The problem under consideration is outlined in Fig. 1. A range-independent ocean environment, bounded above by a possible ice cover and below by a stratified, elastic bottom, is assumed to be interrupted by a local deviation from the ideal, horizontal stratification, in the following referred to as a *facet*. Such facets can be ice keels or grooves in an arctic ice cover or seamounts and diapirs in the ocean bottom. To enable analysis of the forward and backward scattering and

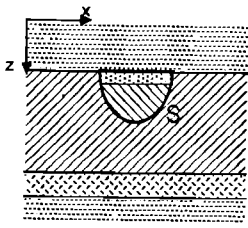


FIG. 1. A horizontally stratified ocean seismoacoustic environment is interrupted by a region of different properties, bounded by the surface  $S$  and stratified as well, although not necessarily with horizontal interfaces as indicated here. A  $(z, x)$  coordinate system is introduced with the  $z$  axis perpendicular to the interfaces in the stratification.

reverberation introduced by such facets, we assume the facet to be sufficiently local to be enclosed within a surface  $S$ , outside which the environment is horizontally stratified. The inner region is assumed to be horizontally stratified as well, but it could be of any composition, provided a mathematical/numerical model for its dynamic behavior is available. Thus the interior could be a structure, modeled by a finite element method, for example. The facet is assumed to have infinite extent in the  $y$  direction and only line sources parallel to the facet will be considered, allowing for a two-dimensional plain strain formulation of the wave equation.

## II. BOUNDARY INTEGRAL FIELD REPRESENTATION

The wave field in an elastic medium is described by the body forces  $\mathbf{f}_i$ , the surface tractions  $\mathbf{t}_i$ , and the displacements  $\mathbf{u}_i$ .

In the frequency domain, the reciprocity theorem of elasticity states that if two distinct elastic fields of time dependence  $\exp(i\omega t)$ ,  $(\mathbf{f}_i^*, \mathbf{t}_i^*, \mathbf{u}_i^*)$  and  $(\mathbf{f}_i, \mathbf{t}_i, \mathbf{u}_i)$  exist in a volume  $V$  bounded by a surface  $S$ , then the work of the forces of the first system  $(*)$  on the displacements of the second is equal to the work done by the forces of the second system on the displacements of the first  $(*)$ ,

$$\int_S \mathbf{t}_i^* \cdot \mathbf{u}_i \, dS + \int_V \mathbf{f}_i^* \cdot \mathbf{u}_i \, dV = \int_S \mathbf{t}_i \cdot \mathbf{u}_i^* \, dS + \int_V \mathbf{f}_i \cdot \mathbf{u}_i^* \, dV. \quad (1)$$

Assuming the first field  $(\mathbf{f}_i^*, \mathbf{t}_i^*, \mathbf{u}_i^*)$  is due to a unit force at a point  $\mathbf{x}'$  inside the volume,  $\mathbf{f}_i^* = \delta_i(\mathbf{x} - \mathbf{x}')$ , then  $\mathbf{t}_i^*$  and  $\mathbf{u}_i^*$  correspond to the Green's functions  $H_{ji}(\mathbf{x}, \mathbf{x}'; \mathbf{n}_S)$  for tractions on a face with outgoing normal  $\mathbf{n}_S$  and  $G_{ji}(\mathbf{x}, \mathbf{x}')$  for displacements at point  $\mathbf{x}$ . Insertion in Eq. (1) then yields

$$\begin{aligned} u_i(\mathbf{x}) + \int_S H_{ji}(\mathbf{x}_S, \mathbf{x}; \mathbf{n}_S) u_j(\mathbf{x}_S) \, dS \\ = \int_S G_{ji}(\mathbf{x}_S, \mathbf{x}) t_j(\mathbf{x}_S; \mathbf{n}_S) \, dS \\ + \int_V G_{ij}(\mathbf{x}, \mathbf{x}_V) f_j(\mathbf{x}_V) \, dV, \end{aligned} \quad (2)$$

where  $u_j(\mathbf{x}_S)$  and  $t_j(\mathbf{x}_S; \mathbf{n}_S)$  are the  $x_j$  components of displacements and tractions on the surface  $S$ , respectively.  $G_{ji}(\mathbf{x}_S, \mathbf{x})$  is the displacement in the  $x_j$  direction at  $\mathbf{x}_S$  due to a force in the  $x_i$  direction at  $\mathbf{x}$  and  $H_{ji}(\mathbf{x}_S, \mathbf{x}; \mathbf{n}_S)$  is the traction in the  $x_j$  direction at the point  $\mathbf{x}_S$  on the surface  $S$  with

outgoing normal  $\mathbf{n}_S$ , due to a force in the  $x_i$  direction at a point  $\mathbf{x}$  inside the volume.

Letting the surface  $S$  correspond to the boundaries of the volume with known boundary conditions, and letting the field point  $\mathbf{x}$  approach a point  $\mathbf{x}'_S$  the boundary, Eq. (2) yields an integral equation for the boundary displacements and tractions,

$$\begin{aligned} u_i(\mathbf{x}'_S) = \oint_S [G_{ji}(\mathbf{x}_S, \mathbf{x}'_S) t_j(\mathbf{x}_S; \mathbf{n}_S) \\ - H_{ji}(\mathbf{x}_S, \mathbf{x}'_S; \mathbf{n}_S) u_j(\mathbf{x}_S)] \, dS \\ + \int_V G_{ij}(\mathbf{x}'_S, \mathbf{x}_V) f_j(\mathbf{x}_V) \, dV. \end{aligned} \quad (3)$$

Equation (3) is valid only for points  $\mathbf{x}'_S$  inside the volume. Therefore, the surface integral must enclose the singularity of the traction Green's function  $H_{ji}(\mathbf{x}_S, \mathbf{x}'_S; \mathbf{n}_S)$  at  $\mathbf{x}'_S = \mathbf{x}_S$ . However, the integration around the singularity can be performed explicitly, modifying the integral equation to

$$\begin{aligned} C_{ij} u_j(\mathbf{x}'_S) = \int_S [G_{ji}(\mathbf{x}_S, \mathbf{x}'_S) t_j(\mathbf{x}_S; \mathbf{n}_S) \\ - H_{ji}(\mathbf{x}_S, \mathbf{x}'_S; \mathbf{n}_S) u_j(\mathbf{x}_S)] \, dS \\ + \int_V G_{ij}(\mathbf{x}'_S, \mathbf{x}_V) f_j(\mathbf{x}_V) \, dV, \end{aligned} \quad (4)$$

where the surface integral is interpreted as the Cauchy principle value, and for a smooth boundary,

$$C_{ij} = \delta_{ij}/2. \quad (5)$$

After solving Eq. (4) for the boundary tractions and displacements, the displacements at any point can be found from Eq. (3), and the associated stresses follow from Hooke's law.

In general, the surface integral must cover all boundaries enclosing the volume, making closed form solution of Eq. (4) impossible for all but trivial problems. Numerical implementation is therefore the only alternative, requiring discretization of the boundary  $S$ , which is the basis for the boundary element method. However, many problems in ocean acoustics and seismology involve boundaries of significant—often infinite—extent.

The discrete wave number approach of Bouchon and Aki<sup>11</sup> overcomes this problem by assuming periodicity in the problem, in combination with the use of a complex frequency formulation. However, the number of discretization points required for typical long range ocean acoustics problems becomes excessive using this approach, at significant computational cost.

However, the Green's functions in Eq. (3) can be chosen arbitrarily provided they satisfy the wave equation in the entire volume. It is easily shown that the surface integral will always vanish along parts of the boundary where the chosen Green's functions satisfy the prescribed boundary conditions. For typical ocean acoustic problems where the environment is globally horizontally stratified but with local facets such as ice keels, subbottom faults, and diapirs, we can therefore limit the surface integral to cover only the facet, provided the Green's function used in the formulation satisfies all boundary conditions in the stratification. This. to-

gether with the fact that efficient numerical codes are available for finding the Green's functions for stratified ocean seismoacoustic environments, makes such an approach an efficient alternative to finite element and finite difference approaches, in particular for long-range scattering and reverberation problems. Further, due to the discretization being limited to the boundary of the facet, this approach is the most suitable for three-dimensional facet reverberation, allowing analysis of out-of-plane scattering from finite ice keels, bottom diapirs, etc.

### III. BOUNDARY ELEMENT FORMULATION

In the following, we describe the discretization of the integral equation, Eq. (4), for two-dimensional, plane strain problems.

#### A. Exterior region

Assuming the exterior medium bounded by the surface  $S$  is plane stratified, a Cartesian coordinate system  $\mathbf{x} = (x_1, x_2) = (z, x)$  is introduced, with the  $z$  axis perpendicular to the stratification, Fig. 1.

We will here use collocation for discretizing Eq. (4). The boundary  $S$  is approximated by  $M$  linear segments, or elements, connected in  $M$  nodes, with node number  $m$  at  $\mathbf{x}^m$  connecting elements number  $m$  and  $m + 1$  as indicated in Fig. 2. Note that we will use a superscript  $m$  to indicate node number and a subscript  $m$  to indicate element number in the following. With the normal pointing away from the volume of interest, i.e., into the inclusion for the outer domain, denoted  $\mathbf{n}_m = (\cos \theta_m, \sin \theta_m)$ , a local coordinate system  $y \in [-1, 1]$  is introduced for the element, Fig. 2, yielding the parameter representation for the coordinates of points on the element,

$$\begin{Bmatrix} z_m(y) \\ x_m(y) \end{Bmatrix} = \begin{Bmatrix} z_m^c \\ x_m^c \end{Bmatrix} + \frac{l_m}{2} \begin{Bmatrix} -\sin \theta_m \\ \cos \theta_m \end{Bmatrix} y, \quad (6)$$

with  $\mathbf{x}_m^c = (z_m^c, x_m^c)$  being the coordinates for the center point of the element and  $l_m$  being the length of the element.

The distribution of displacements and stresses along the element are now assumed to be in the form

$$\begin{Bmatrix} \mathbf{u}(y) \\ \mathbf{t}(y) \end{Bmatrix} = \begin{Bmatrix} \mathbf{u}^{m-1} \\ \mathbf{t}^{m-1} \end{Bmatrix} N(y) + \begin{Bmatrix} \mathbf{u}^m \\ \mathbf{t}^m \end{Bmatrix} N(-y), \quad (7)$$

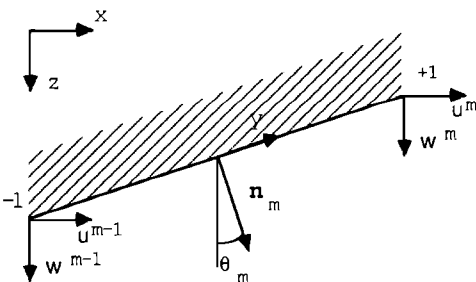


FIG. 2. Boundary element notation. Element  $m$  interconnects nodes  $m - 1$  and  $m$  and has the normal  $\mathbf{n}_m = (\cos \theta_m, \sin \theta_m)$  pointing away from the volume  $V$  of interest. A local coordinate system  $y \in [-1, 1]$  is introduced for the element, as indicated.

with  $\mathbf{u}^m, \mathbf{t}^m$  being the displacements and tractions in node number  $m$ , and  $N(y)$  being a linear interpolation function,

$$N(y) = (1 - y)/2. \quad (8)$$

Insertion of Eq. (7) now yields the following discrete form of Eq. (4):

$$\begin{aligned} \bar{C}^n u_i^n &= \sum_{m=1}^M \sum_{j=1}^2 [G_{ji}^{mn} t_j^m - H_{ji}^{mn} u_j^m] + \hat{u}_i^n, \\ n &= 1, \dots, M, \quad i = 1, 2, \end{aligned} \quad (9)$$

where  $\hat{u}_i^n$  is obtained from the volume integral in Eq. (4), representing the source contribution to the node displacements, and  $G_{ji}^{mn}$  and  $H_{ji}^{mn}$  are the influence matrices

$$\begin{aligned} G_{ji}^{mn} &= \frac{l_m}{2} \int_{-1}^1 G_{ji}(\mathbf{x}_m(y), \mathbf{x}^n) N(-y) dy \\ &+ \frac{l_{m+1}}{2} \int_{-1}^1 G_{ji}(\mathbf{x}_{m+1}(y), \mathbf{x}^n) N(y) dy, \end{aligned} \quad (10)$$

$$\begin{aligned} H_{ji}^{mn} &= \frac{l_m}{2} \int_{-1}^1 H_{ji}(\mathbf{x}_m(y), \mathbf{x}^n, \mathbf{n}_m) N(-y) dy \\ &+ \frac{l_{m+1}}{2} \int_{-1}^1 H_{ji}(\mathbf{x}_{m+1}(y), \mathbf{x}^n, \mathbf{n}_{m+1}) N(y) dy. \end{aligned} \quad (11)$$

#### B. Combining two regions

For homogeneous boundary conditions  $u_j^m = 0$  or  $t_j^m = 0$ , the BEM equations, Eq. (9), can be solved for the unknown node tractions or displacements, respectively. For the inclusion being elastic, the boundary element equations must be set up for the interior of the inclusion, now with the surface normal pointing out into the exterior region,

$$\begin{aligned} \bar{C}^n \bar{u}_i^n &= \sum_{m=1}^M \sum_{j=1}^2 [\bar{G}_{ji}^{mn} \bar{t}_j^m - \bar{H}_{ji}^{mn} \bar{u}_j^m] + \bar{u}_i^n, \\ n &= 1, \dots, M, \quad i = 1, 2. \end{aligned} \quad (12)$$

The node displacements and tractions in the two regions must now satisfy the continuity conditions,

$$\bar{\mathbf{u}}^m = \mathbf{u}^m, \quad (13)$$

$$\bar{\mathbf{t}}^m = -\mathbf{t}^m, \quad (14)$$

which, inserted into Eq. (12), yield

$$\begin{aligned} \bar{C}^n u_i^n &= \sum_{m=1}^M \sum_{j=1}^2 (-\bar{G}_{ji}^{mn} t_j^m - \bar{H}_{ji}^{mn} u_j^m) + \bar{u}_i^n, \\ n &= 1, \dots, M, \quad i = 1, 2. \end{aligned} \quad (15)$$

Equations (9) and (15) now form a system of linear equations that can be solved for the node tractions and displacements,

$$\begin{bmatrix} \mathbf{H} & -\mathbf{G} \\ \bar{\mathbf{H}} & \bar{\mathbf{G}} \end{bmatrix} \begin{bmatrix} \mathbf{u} \\ \mathbf{t} \end{bmatrix} = \begin{bmatrix} \hat{\mathbf{u}} \\ \bar{\mathbf{u}} \end{bmatrix}. \quad (16)$$

#### C. Influence functions

The kernel  $G_{ji}(\mathbf{x}_m(y), \mathbf{x}^n)$  represents the displacement in the  $x_j$  direction at a point  $\mathbf{x}_m(y)$  on element  $m$ , due to a virtual unit force in the  $x_i$  direction at the node at  $\mathbf{x}^n$  for the exterior layered medium without the facet. Similarly, the

kernel  $H_{ji}(\mathbf{x}_m(y), \mathbf{x}^n; \mathbf{n}_m)$  represents the  $x_j$  component of the tractions on the  $m$ th element with outgoing normal  $\mathbf{n}_m$ .

Since both the inner and outer domains separated by the boundary  $S$  are assumed to be plane stratified, the Green's functions are most conveniently determined by separation of variables through integral transforms. The theory for propagation in plane stratified media is well established,<sup>25,26</sup> and several numerical schemes have been developed for the solution, including various forms of the propagator matrix approach of Thomson<sup>27</sup> and Haskell,<sup>28</sup> the invariant embedding approach of Kennen,<sup>10</sup> the discrete wave number method by Bouchon and Aki,<sup>11</sup> and the direct global matrix (DGM) method of Schmidt.<sup>12,24</sup> The DGM approach inherently solves for multiple sources and receivers simultaneously for arbitrary fluid/solid stratifications, and is therefore well suited for computation of the kernels of Eq. (4). We will here use a modified version of the DGM SAFARI code,<sup>29</sup> incorporating multiple sources and analytical integration of the Green's functions over the boundary elements. The use of SAFARI is convenient since it retains all features of the existing code, including the mixed fluid/solid stratifications characteristic of ocean acoustic reverberation problems, as well as special features such as transverse isotropy<sup>30</sup> and interface roughness.<sup>5</sup>

### 1. Green's functions for stratified media

Here, only an outline of the DGM approach will be given, focusing on the details pertinent to the present BEM formulation; for further details, reference is made to the published literature.<sup>12,24</sup> The displacements and stresses of time dependence  $\exp(i\omega t)$  are, in vector form,

$$\mathbf{f}(\mathbf{x}) = \begin{Bmatrix} u_i(\mathbf{x}) \\ \sigma_{ij}(\mathbf{x}) \end{Bmatrix}. \quad (17)$$

The tractions on a surface with outgoing normal  $\mathbf{n}$ , needed in the BEM formulation, are determined from the stress tensor by the relation

$$t_i(\mathbf{x}; \mathbf{n}) = \sigma_{ij}(\mathbf{x}) n_j(\mathbf{x}). \quad (18)$$

The solution for a stratified medium is based on the integral transform representation of the Green's function, for plane strain the Fourier transform,

$$\mathbf{f}(\mathbf{x}, \mathbf{x}') = \int_{-\infty}^{\infty} \tilde{\mathbf{f}}(z, z'; k) e^{-ik(x-x')} dk, \quad (19)$$

$$\tilde{\mathbf{f}}(z, z'; k) = \frac{1}{2\pi} \int_{-\infty}^{\infty} \mathbf{f}(\mathbf{x}, \mathbf{x}') e^{ik(x-x')} dx, \quad (20)$$

with  $\mathbf{x} = (z, x)$  being the field point,  $\mathbf{x}' = (z', x')$  the source point, and the depth-dependent Green's function  $\tilde{\mathbf{f}}(z, z'; k)$  satisfying an ordinary differential equation in depth, the so-called depth-separated wave equation.

The DGM approach solves the depth-separated wave equation by expressing the total Green's function in layer number  $m$  as a superposition of the free-field Green's function for sources in the layer, and solutions to the homogeneous wave equation,

$$\tilde{\mathbf{f}}_l(z, z'; k) = \hat{\mathbf{f}}_l(z, z'; k) + \tilde{\mathbf{f}}_l^*(z; k), \quad (21)$$

where both the source contribution  $\hat{\mathbf{f}}_l(z, z'; k)$  and the homo-

geneous solution  $\tilde{\mathbf{f}}_l^*(z; k)$  in an elastic layer are of the form

$$\tilde{\mathbf{f}}_l^*(z; k) = \mathbf{K}_l(k) \mathbf{E}_l(z, k) \mathbf{A}_l(k), \quad (22)$$

where  $\mathbf{K}(k)$  is a coefficient matrix, a function of wave number  $k$  only and  $\mathbf{E}_l(z, k)$  is a diagonal matrix containing all depth dependence,

$$\mathbf{E}_l(z, k) = \text{diag} [ e^{-\alpha z}, e^{-\beta z}, e^{-\alpha z'}, e^{-\beta z'} ], \quad (23)$$

with  $z^- = z - z_{l-1}$ ,  $z^+ = z_l - z$  being the distances from the field point to the interfaces bounding the layer above and below, respectively, and

$$\alpha = \sqrt{k^2 - h_l^2}, \quad \beta = \sqrt{k^2 - \kappa_l^2}, \quad (24)$$

with  $h_l$  and  $\kappa_l$  being the wave numbers for compression and shear, respectively, and  $\mathbf{A}_l(k)$  is a vector containing the wave field amplitudes, known for the source contribution and to be determined from the boundary conditions for the homogeneous solution.

The boundary conditions to be satisfied simultaneously at all horizontal interfaces then take the form

$$\begin{aligned} \tilde{\mathbf{f}}_l^*(z_l; k) - \tilde{\mathbf{f}}_{l-1}^*(z_l; k) \\ = \hat{\mathbf{f}}_{l-1}(z_l; k) - \hat{\mathbf{f}}_l(z_l; k), \quad l = 1 \dots (M-1), \end{aligned} \quad (25)$$

i.e., a global system of linear equations in the wave field amplitudes  $\mathbf{A}_l(k)$ , the solution of which is unconditionally stable with the particular choice of local coordinate systems used in the depth solutions, Eq. (23). Once solved, the solution vector  $\mathbf{A}_l(k)$  is inserted into Eq. (22) and superposed with the source contributions, and the displacement and stress components of the Green's function are determined at any depth in the stratification through evaluation of the Fourier transforms, Eq. (19), with the tractions following from Eq. (18). Further, the source contributions only appear on the right-hand side of Eq. (25). Multiple sources can therefore be treated simply by adding multiple right-hand sides, enabling the determination of all kernels in Eqs. (10) and (11) with one solution of Eq. (25). This feature of the hybrid DGM-BEM approach is the main reason for the numerical efficiency of the present approach.

To determine the influence functions, the element integrations in Eqs. (10) and (11) must be performed. This can of course be done by numerical quadrature, requiring proper sampling of the Green's functions over the elements. However, the present wave number representation of the kernels allows for closed form evaluation of the element integrals. This is described in the following section.

### 2. Element integration

The components of the Green's functions to be integrated over the elements in Eqs. (10) and (11) are obtained by evaluation of the integral over wave number, Eq. (19), of the kernels obtained from the DGM solution.

The integrations to be performed in Eqs. (10) and (11) are therefore of the form

$$\begin{aligned} I_m^\pm = \frac{l_m}{2} \int_{-1}^1 \left( \int_{-\infty}^{\infty} \tilde{\mathbf{f}}(z_m(y), z''; k) \right. \\ \left. \times e^{-ik(x_m(y) - x'')} dk \right) \mathcal{N}(\pm y) dy. \end{aligned} \quad (26)$$

Insertion of Eq. 22 and interchange of the integrations yield

$$I_m^\pm = \frac{l_m}{2} \int_{-\infty}^{\infty} \mathbf{K}(k) \left( \int_{-1}^1 \mathbf{E}(z_m(y), k) \times e^{-ik(x_m(y) - x^n)} N(\pm y) dy \right) \mathbf{A}(k) dk. \quad (27)$$

If we choose the interpolation function as a linear combination Legendre function,

$$N(y) = \sum_n a_n P_n(y), \quad (28)$$

and use the identity<sup>31</sup>

$$\int_{-1}^1 P_n(y) e^{iRy} dy = 2i^n j_n(R), \quad (29)$$

where  $j_n$  is the spherical Bessel function of order  $n$ , then the inner integration can be performed in closed form.

For the present linear variation over the elements,

$$N(y) = (P_0(y) - P_1(y))/2. \quad (30)$$

Insertion of the parameter representation for the element coordinates, Eq. (6), then yields

$$I_m^\pm = l_m \int_{-\infty}^{\infty} \mathbf{K}(k) \mathbf{J}_m^\pm(k) \mathbf{E}(z_m^c, k) \mathbf{A}(k) e^{-ik(x_m^c - x^n)} dk, \quad (31)$$

where  $\mathbf{J}_m^\pm(k)$  is the diagonal matrix,

$$\mathbf{J}_m^\pm(k) = \text{diag} \begin{bmatrix} j_0((-i\alpha s_m - kc_m)(l_m/2)) \pm ij_1((-i\alpha s_m - kc_m)(l_m/2)) \\ j_0(-i\beta s_m - kc_m)(l_m/2) \pm ij_1(-i\beta s_m - kc_m)(l_m/2) \\ j_0(i\alpha s_m - kc_m)(l_m/2) \pm ij_1(i\alpha s_m - kc_m)(l_m/2) \\ j_0(i\beta s_m - kc_m)(l_m/2) \pm ij_1(i\beta s_m - kc_m)(l_m/2) \end{bmatrix}, \quad (32)$$

with  $(c_m, s_m) = (\cos \theta_m, \sin \theta_m)$ .

It is now clear from the form of Eq. (31) that the element integration can be accounted for simply by modifying the wave number kernels computed by SAFARI by multiplication with the element length and the diagonal matrix in Eq. (32).

#### D. Field computation

Once the nodal displacements have been determined by solving the BEM equations (16), the field in the external region is determined from the discretized integral representation,

$$u_i(\mathbf{x}) = \sum_{m=1}^M \sum_{j=1}^2 [G_{ji}^m(\mathbf{x}) t_j^m - H_{ji}^m(\mathbf{x}) u_j^m] + \hat{u}_i(\mathbf{x}), \quad i = 1, 2, \quad (33)$$

similar to Eq. (9), but with the node  $\mathbf{x}^n$  replaced by the field point  $\mathbf{x}$ . The stresses follow from Hooke's law, applied at the field point  $\mathbf{x}$ .

We could now use SAFARI to compute the Green's functions in Eq. (33) for each of  $N$  desired receiver depths, requiring computation of  $2 \times M \times N$  Green's functions for each combination of the coordinate indices  $ij$ . Further, in cases where the field in a fluid layer has to be computed, we would have to establish a reciprocity theorem for combined fluid/solid regions.<sup>32</sup> In such cases, Eq. (1) is not directly applicable since point forces cannot be applied in fluid media. However, we can modify Eq. (33) to be more numerically efficient and more important directly allowing for computation of the field everywhere in a fluid/solid stratification.

As is clear from the form of the field representation, Eq. (33), the surface integral is equivalent to a source distribution. We can therefore apply it as such in the superposition principle of the DGM approach, where the total field within

a layer is a sum of the free-field source contributions in the layer and a solution satisfying the homogeneous wave equation. Equation (33) is therefore reformulated such that all parts of the solution satisfying the homogeneous wave equation in layer  $l$  are collected in the term  $u_i^*(\mathbf{x})$ . These include all contributions from sources and elements in other layers as well as the field reflected off the horizontal boundaries of the layer. Equation (33) then takes the form

$$u_i(\mathbf{x}) = \sum_{m=1}^{M_l} \sum_{j=1}^2 [\hat{G}_{ji}^m(\mathbf{x}) t_j^m - \hat{H}_{ji}^m(\mathbf{x}) u_j^m] + \hat{u}_i(\mathbf{x}, \mathbf{x}') + u_i^*(\mathbf{x}), \quad i = 1, 2, \quad (34)$$

where  $\hat{G}_{ji}^m(\mathbf{x})$  and  $\hat{H}_{ji}^m(\mathbf{x})$  are now the free-field influence functions, and  $\hat{u}_i(\mathbf{x}, \mathbf{x}')$  are the displacements corresponding to the free-field Green's function for the physical sources within the layer. The summation obviously includes only the  $M_l$  nodes that are present in the actual layer. The term  $u_i^*(\mathbf{x})$  represents a yet unknown homogeneous solution to be determined from the boundary conditions at the horizontal interfaces. Since the field in each layer is now expressed as a superposition of free-field source terms (elements and physical sources) and an unknown homogeneous solution, we can use the DGM approach to solve for the homogeneous solution.

We insert the known wave number representation for the free-field Green's functions and perform the element integrations analytically as described above to yield

$$u_i(\mathbf{x}) = \sum_{m=1}^{M_l} \sum_{j=1}^2 \int_{-\infty}^{\infty} [\hat{g}_{ji}^m(z_m^c, z; k) t_j^m - \hat{h}_{ji}^m(z_m^c, z; k) u_j^m] \times e^{-ik(x_m^c - x)} dk + \hat{u}_i(\mathbf{x}, \mathbf{x}') + u_i^*(\mathbf{x}), \quad i = 1, 2. \quad (35)$$

We then apply the forward Fourier transform, Eq. (20) with  $k$  replaced by  $k'$ , to Eq. (35) together with the identity

$$\frac{1}{2\pi} \int_{-\infty}^{\infty} e^{ix(k+k')} dx = \delta(k+k'), \quad (36)$$

and obtain the wave number kernels for the displacement at the receiver depth  $z$ ,

$$\begin{aligned} \bar{u}_i(z;k) = & \sum_{m=1}^{M_i} \sum_{j=1}^2 e^{ikx'_m} [\hat{g}_{ji}(z'_m, z; -k) t_j^m \\ & - \hat{h}_{ji}(z'_m, z; -k) u_j^m] + \hat{u}_i(z, z'; k) \\ & + \bar{u}_i^*(z;k), \quad i = 1, 2. \end{aligned} \quad (37)$$

The corresponding wave number kernels for the stress at depth  $z$  are now found from Hooke's law. In the wave number domain, the spatial variation of the free-space Green's function is known; thus we obtain the spatial derivatives of the displacements involved in Hooke's law by algebraic operations in Eq. (37), yielding the displacement-stress vector,

$$\bar{\mathbf{f}}(z;k) = \begin{Bmatrix} \bar{u}_i(z;k) \\ \bar{\sigma}_{ij}(z;k) \end{Bmatrix} = \hat{\mathbf{f}}_i(z;k) + \bar{\mathbf{f}}_i^*(z;k), \quad (38)$$

where the "source" term  $\hat{\mathbf{f}}_i(z;k)$  is a superposition of the contributions from the physical sources and the boundary elements within layer  $i$ . The homogeneous solution  $\bar{\mathbf{f}}_i^*(z;k)$  is of the form given in Eq. (21), with the plane-wave amplitudes  $A_i(k)$  being unknown.

By determining the source terms and the coefficients to the homogeneous solution at the horizontal boundaries of the layer,  $z = z_{i-1}$  and  $z = z_i$ , we have all terms needed for the DGM equations, Eq. (25), the solution of which determines the unknown wave field amplitudes  $A_i(k)$  in all layers, fluid or solid, simultaneously, and the total field can then be determined by evaluating the backward Fourier transform of Eq. (37).

In addition to automatically determining the field in any fluid or elastic layer in the stratification, this approach is more efficient since all source and element terms in the wave number kernels for the physical sources and element contributions in Eq. (37) are simply superimposed, requiring only one right-hand side in the global matrix equations (25).

## E. Numerical considerations

Although the influence matrices of the BEM equations, Eq. (9), are straightforward computed by means of a slightly modified SAFARI code as described above, there are several numerical issues that must be considered. Some of these issues are of general nature for wave number integration algorithms and some are introduced in particular for the BEM formulation, requiring computation of extremely short-range Green's functions.

### 1. Green's function singularities

The Green's functions  $H_{ji}(\mathbf{x}_S, \mathbf{x}'_S; \mathbf{n}_S)$  for tractions have a  $|\mathbf{x}_S - \mathbf{x}'_S|^{-1}$  singularity that must be enclosed by the surface integration in Eq. (3). This can be accomplished by interpreting the integral as the Cauchy principal value and explicitly adding the contribution from a contour encircling the singularity. This is illustrated in Fig. 3, showing node number  $m$  connecting elements number  $m$  and  $m+1$ . The

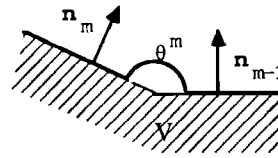


FIG. 3. Integration contour for singular contribution. The volume  $V$  is indicated by the hatched area.

singularity is encircled by a small circular arc of radius  $\epsilon$ . If the arc was encircling the singularity entirely, the contour integral would be  $-1$ . For the present angle,  $\theta^m = \pi - (\theta_{m+1} - \theta_m)$ , we assume a proportional contribution,

$$\Delta I^m = -[\pi - (\theta_{m+1} - \theta_m)]/2\pi, \quad (39)$$

yielding the following expression for the factor  $C''$  in Eq. (9):

$$C'' = 1 + \Delta I'' = [\pi + (\theta_{m+1} - \theta_m)]/2\pi, \quad (40)$$

which for a node with no change in element angle translates to a factor of  $C'' = 1/2$ .

### 2. Wave number integration

The numerical evaluation of the wave number integrals is a critical point for wave number integration approaches. There are two critical issues to consider. One is the truncation of the wave number integration interval, and the other is the wave number sampling.<sup>29</sup>

To obtain an accurate solution, it is necessary to truncate the wave number integration at a point where the eliminated integral to infinity is negligible. A proper choice is therefore closely linked to the asymptotic behavior of the kernels for  $k \rightarrow \pm \infty$ . For large wave numbers, the weakest decay of the free-field integrands of the backward Fourier transform, Eq. (19), is of the form

$$\bar{f}(z, z'; k) e^{ikx} \sim k^{-1} e^{-k|z-z'|} e^{ikx}. \quad (41)$$

The analytical integration over the element has increased the convergence by  $k^{-1}$  as opposed to a simple boundary integral representation. For cases where source and receivers are at different depths, the exponential function usually ensures a rapid conversion, making it sufficient to include wave numbers slightly higher than the largest wave number in the environment. For source and receiver at the same depth, the existence of the integral is ensured only by cancellation through the multiplication with the exponential function in range  $x$ , and here the truncation becomes a critical issue. An abrupt truncation will always give rise to truncation errors. However, this problem can be overcome by tapering the kernel over a wave number interval where the exponential function oscillates through several periods,<sup>29</sup> ensuring proper cancellation. The actual choice of tapering interval is obviously dependent on the range  $x$  separating source and receiver. In traditional waveguide computations, the range is usually relatively large compared to the wavelength, making tapering of the highest 10% of the wave numbers sufficient. However, in the present case the computation of the element influence matrices involves extremely short ranges as well as small depth separations, requiring substantially more tapering. The actual numerical

values will be discussed in relation to the examples following in the next section.

The wave number sampling is traditionally a critical issue for wave number integration algorithms. However, it is relatively straightforward to determine a sufficient sampling through the sampling theorem in combination with choosing a complex wave number integration contour, as described in detail in Ref. 29. In summary, the wave number sampling interval  $\Delta k$  should satisfy the inequality

$$\Delta k < 2\pi/aR, \quad (42)$$

where  $R$  is the maximum range of interest and  $a$  is a factor which should be at least 2.0 for cases involving the spectrum for negative wave numbers. A value of  $a = 3.0$  has been found empirically to be sufficient for all practical purposes. However, this sampling is not sufficient to ensure correct results. The discrete integration will still give rise to wrap-around of the field outside the range window  $aR$ . This wrap-around is reduced by choosing a complex wave number contour for evaluation of the inverse Fourier transform, Eq. (19).

In setting up the BEM equations, Eq. (9), we need to determine extremely short-range influence functions as well as long-range Green's functions for the field produced on the facet boundary by the physical sources. According to the above discussion, we therefore need a large wave number interval for the influence functions, but with weak sampling requirements, whereas the sampling requirements are stricter for the source field, over a much smaller wave number interval, however.

It is therefore convenient to separate the wave number computation and integration for the two components, in spite of the fact that the DGM approach could solve for both simultaneously. For the same reason, the Green's function computations needed for the received field are also performed as a separate computation, allowing adjustment of the sampling parameters to the receiver positions of interest. The splitting of the Green's function computations in three independent parts also has the advantage that the computationally most intensive part, the evaluation of the influence functions, can be performed just once for a particular environment, and reused for several source-receiver scenarios.

In summary, the basic algorithm can be separated into five distinct parts:

- (1) Computation of exterior influence function [Eqs. (10) and (11)].
- (2) Computation of interior influence function [Eqs. (10) and (11)].
- (3) Computation of source contribution to nodal displacements [ $\hat{u}$  in Eq. (16)].
- (4) Solve the BEM system of equations [Eq. (16)].
- (5) Computation of the scattered field [Eq. (37)].

Parts 1, 2, 3, and 5 each represent a SAFARI run. For parts 1 and 2, the computation involves a number of independent sources corresponding to two times the number of nodes. For an inclusion with homogeneous boundary conditions, part 2 is not necessary. We roughly estimate a BEM computation will take from 3–10 times the CPU time of a normal SAFARI run, depending on the number of nodes.

### 3. Time domain solutions

For time domain solutions obtained by Fourier synthesis, the frequency sampling is a critical issue. However, in analogy to the wave number sampling, wraparound can be eliminated by evaluating the Fourier series along a complex frequency contour. When using complex frequency, it is not necessary also to use complex wave number. Complex frequency has been used in all time domain solutions following.

## IV. NUMERICAL EXAMPLES

To illustrate the efficiency and versatility of the hybrid DGM-BEM approach for simulation of ocean seismoacoustic reverberation, we will apply it to three different reverberation scenarios. The first is a simple benchmark problem, which will be used to illustrate the correctness of the solution. The second problem concerns the long-range reverberation produced by a groove in the ice sheet covering an Arctic Ocean environment with a realistic sound-speed profile. The last example simulates the short-range reverberation from an elastic bottom facet in the time domain.

### A. Semicircular canyon in elastic half-space

To evaluate the performance of the DGM-BEM approach, we will apply it to the problem used by Kawase<sup>21</sup> to evaluate his approach. A homogeneous elastic half-space

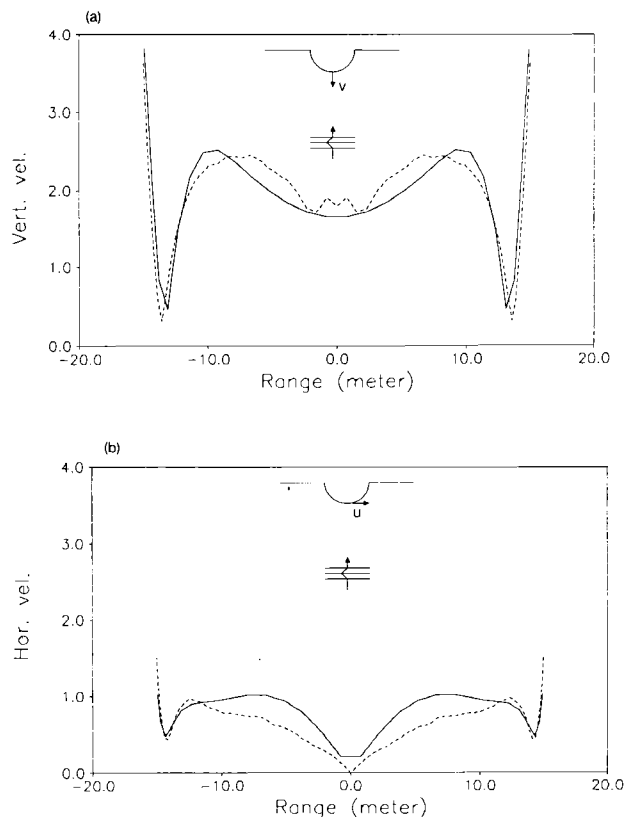


FIG. 4. Displacements at the surface of a semicircular canyon computed by the present approach with 30 elements (solid curve), and by a standard boundary integral method with 60 nodes (dashed curves). The results obtained by the present approach are in perfect agreement with the results of Kawase<sup>21</sup> and Wong.<sup>33</sup> (a) Vertical displacements versus horizontal node position; (b) horizontal displacements.

with shear speed  $c_s$ , Poisson ratio  $\nu = 0.33$  ( $c_p = 2c_s$ ), and density  $\rho$  has a semicircular canyon with radius  $a$ . We determine the vertical and horizontal displacements at the surface of the canyon for a vertically incident, plane  $P$  wave of frequency  $f = c_s/a$ , i.e., with a  $P$  wavelength equal to the diameter of the canyon. The displacement amplitude of the incident wave is unity. We use 30 boundary elements for representing the canyon, and Fig. 4(a) shows the computed vertical node displacements versus the horizontal node position as a solid curve. Figure 4(b) shows the corresponding horizontal displacements. The results are in perfect agreement with the results obtained by Kawase<sup>21</sup> and earlier by Wong.<sup>33</sup> To illustrate the accuracy and efficiency of the present closed form element integration, we have shown the results obtained with a standard boundary integral method with 60 nodes and no element integration as dashed curves. The results of the standard approach have obviously not converged to the correct solution with 60 nodes. Due to the doubling of the number of nodes, the standard solution was obtained at almost four times the computational cost, clearly indicating the efficiency and accuracy of the present approach.

For the actual computation of the influence function, the wave number kernels are sampled with 1024 points for a horizontal phase velocity  $c = \omega/k$  from  $-20$  to  $20$  m/s. For phase velocities lower than  $200$  m/s, tapering has been applied in order to speed up the convergence. However, this is computationally very demanding and an analytical evaluation of this contribution will significantly speed up the computations. An adaptive scheme<sup>34,35</sup> would also significantly improve the speed of the computations.

### B. Reverberation from ice facets

We next address a problem that for computational reasons is prohibitive for discrete methods and that cannot be

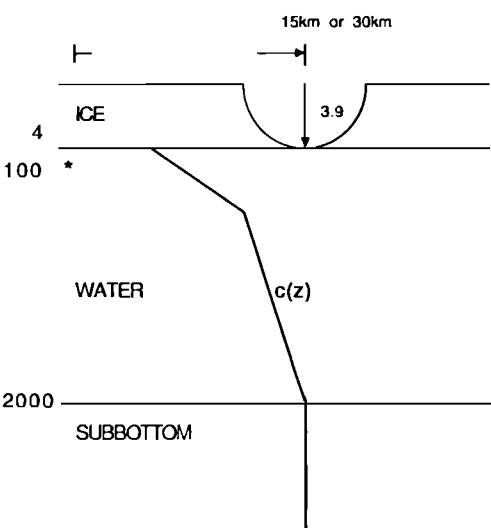


FIG. 5. Arctic environment with a semicircular groove in an elastic ice cover. A canonical bilinear sound-speed profile is assumed in the water column of 2000-m depth. Two different ranges between source and groove are considered, 15 and 30 km.

solved by any of the earlier published BEM approaches due to the fluid-elastic nature of the stratification.

We consider the long-range reverberation from a groove in an ice sheet covering a realistic Arctic Ocean environment. The ice sheet is assumed to be of uniform thickness 4 m, except for the groove that is assumed to be semicircular with radius 3.9 m, almost penetrating the ice as shown in Fig. 5. The compressional and shear speeds of the ice are 3000 and 1600 m/s, respectively, and the density  $0.9$  g/cm<sup>3</sup>. A bilinear sound-speed profile is assumed in the water column of depth 2000 m, with 1435 m/s just below the ice and 1481 m/s at the seabed. The bottom is relatively unimportant for the long-range propagation and reverberation in this case, and we therefore assume it to be a fluid half-space with a sound speed of 1481 m/s.

A 50-Hz acoustic line source is assumed to be placed at a depth of 100 m, producing the field shown as contours in depth and range in Fig. 6(a) in the absence of the ice groove. The contour interval is 3 dB, but the absolute levels are arbitrary. The field clearly exhibits the characteristic surface duct and convergence zone pattern, with the convergence zone distance being approximately 30 km. We now consider

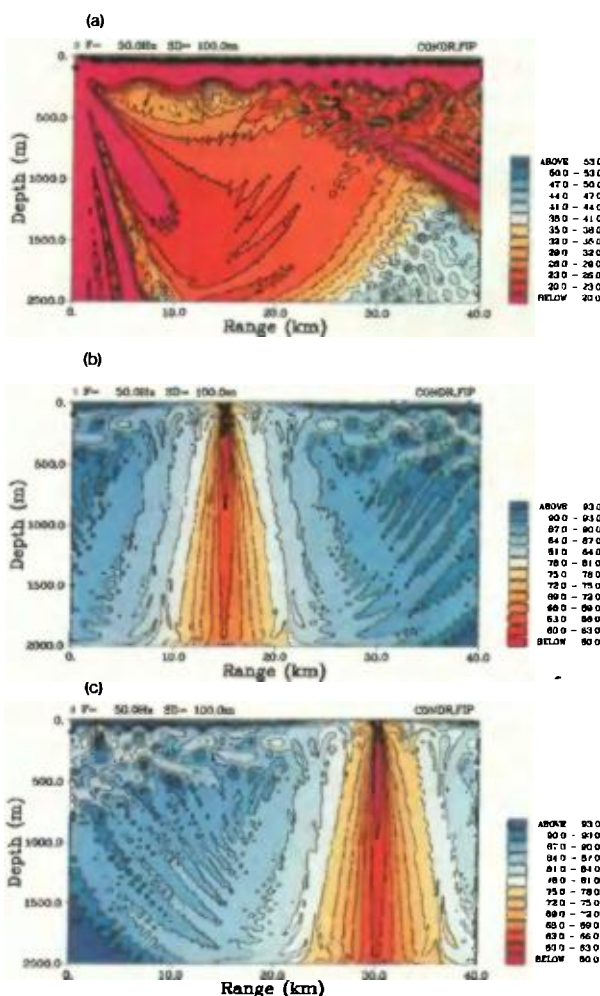


FIG. 6. Contours of acoustic field in an arctic environment for a 50-Hz line source at depth 100 m. Contour interval is 3 dB, but actual levels are arbitrary. (a) Field in absence of groove; (b) field scattered by groove at 15-km range; (c) field scattered by groove at 30-km range.

two positions of the groove, one at 30-km range in the convergence zone and one at 15 km, i.e., half a convergence zone away from the source. The scattered fields produced in the two cases are shown in the form of field contours in Fig. 6(b) and (c).

There are several things to note in the results shown in Fig. 6. First of all, the structure of the scattered field is very similar for the two cases due to the significance of the surface duct propagation, but the levels are in general 3 dB higher for the groove at 30 km due to the convergence zone contribution. Further, because the scattered field itself is dominated by the convergence zone path due to the dominantly vertical angles generated, the reverberation produced on a vertical array in a monostatic scenario is approximately 6 dB higher for the groove at 30-km distance than for the one at 15-km distance. Here, it should of course be pointed out that these considerations ignore geometric spreading associated with more realistic point source scenarios. On the other hand, the issue is signal to noise ratio (SNR), and a target signal will be subject to the same geometric spreading laws. Thus a signal from a target at 100-m depth in the convergence zone will be only a couple of dB higher than for the target at 15-km range (ignoring geometric spreading), but the reverberation from a groove at the same distance is 6 dB higher, translating into a 3- to 4-dB-higher SNR in terms of reverberation for the target and ice facet at 15-km range.

Another important issue is the energy loss induced by scattering into flexural waves in the ice, which when accu-

mulated over many ice facet interactions is suspected to be an important transmission loss mechanism<sup>5</sup> due to the fact that these waves are subsonic and therefore evanescent in the water column. To illustrate this qualitatively and demonstrate the interpretation advantage of the wave field decomposition inherent in the present approach, Fig. 7(a) shows the wave number kernel for the scattered field just below the ice. Both the negative and positive wave number spectrum is shown, with the negative wave numbers corresponding to the backscattered field. The wave numbers  $|k| < 0.2$  correspond to waves propagating in the water column, whereas the larger wave numbers are evanescent in the water column, as can be observed in Fig. 7(b), showing the corresponding wave number kernels at depth 55 m. As may be expected, the propagating components are slightly stronger in the forward direction. However, it is more interesting to note the strength of the scattered flexural waves, represented by the strong peaks in the evanescent regimes. In particular, the relative strength of the backward scattered flexural wave is interesting, a phenomenon that could be addressed in future scattering experiments, in particular if geophone arrays are deployed on the ice.

As the wavelength is much larger than width of the ice groove, the exact shape of the groove is not important. Here, ten elements were used and the sound speed profile was modeled by ten layers with  $c(z)^{-2}$  linear in each layer. The wave number sampling parameters were similar to the ones in the previous examples for computation of the influence function. For the propagation of the scattered field, the wave number kernel was sampled in 1024 points over an interval corresponding to phase velocities between  $-200$  and  $200$  m/s. The total computation time was 3 min on an Alliant FX-40 with two processors.

### C. Reverberation from subbottom facets

As a last example, we will illustrate the versatility of the DGM-BEM approach by simulating the short-range, time domain reverberation from a subbottom elastic facet. The environment is shown in Fig. 8. A cylindric granite inclusion of radius 70 m is embedded in the subbottom of a stratified shallow water environment with water depth 200 m. The bottom consists of a 30-m silt/sand sediment layer overlaying a sand subbottom. The environmental parameters are summarized in Table I.

A transient acoustic source at depths 10 and 400 m from the center of the facet range is transmitting a second-order Blackman-Harris pressure pulse, shown in Fig. 9, with a center frequency of 20 Hz. We compute the acoustic field in the water column over a fine grid in the range window 200–550 m relative to the source, covering both the backscattering and forward scattering regions for the facet.

Figure 10(a) shows the field contours at  $t = 0.35$  s, shortly after the first interaction with the facet. Red color indicates positive stress (negative pressure), and blue indicates negative stress. The incident and bottom bounced wavelets are clearly identifiable, together with the secondary surface bounce. In addition, the facet reverberated wavelet is visible in the bottom left half of Fig. 10(a). Figure 10(b) and (c) shows the field at  $t = 0.40$  s and  $t = 0.45$  s, where the

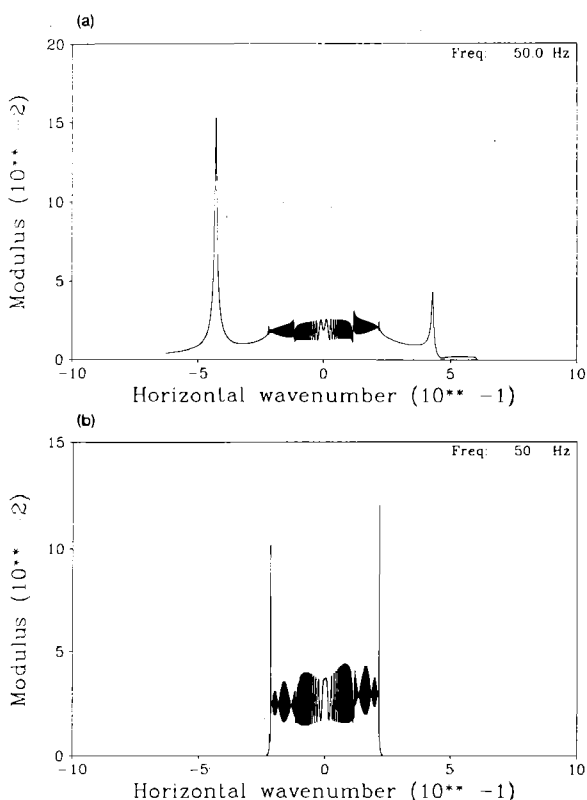


FIG. 7. Wave number kernel for scattered acoustic pressure: (a) below ice cover, at depth 4.0 m; (b) at depth 55 m. Scattering into evanescent flexural wave in ice is evident, in particular in the backward direction (negative wave numbers).

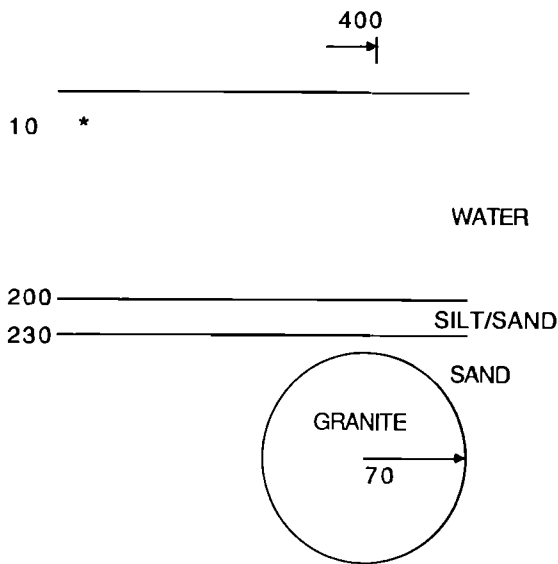


FIG. 8. Cylindric granite inclusion in stratified elastic seabed. Transient source at 10-m depth, 400 m from center of inclusion. Pressure field in water determined over entire water depth, 200 m, between 200- and 550-m range from source.

major wavelets of the incident and scattered wavelets are still visible, but very difficult to interpret in detail.

Here, we can take advantage of the separation of the incident field and the scattered field inherent in the BEM approach, simply by excluding the source term  $\hat{u}_i(z, z'; k)$  in Eq. (37), leaving only the boundary element contributions as source terms in the DGM solution. Figure 11(a), (b), and (c) shows the scattered field alone, at times 0.35, 0.40, and 0.45 s, respectively. Figure 11(b) shows a clear dominance of forward scattering from the facet. However, it is more interesting to note the conversion into shear waves and interface waves induced by the facet, evident in Fig. 11(c). The peaks in the pressure field at the bottom at range 340 m and the negative peak at 450 m correspond to scattered shear body waves and Scholte waves. To illustrate the more detailed time variation of the reverberation, the equivalent time series recorded by a vertical array at 200-m range is shown in stacked format in Fig. 12. Again the primary arrivals are identifiable in the total signals shown in Fig. 12(a),

TABLE I. Environmental parameters for bottom facet problem.

Medium	Compression		Shear		Density g/cm <sup>3</sup>
	Speed m/s	Atten dB/λ	Speed m/s	Atten dB/λ	
Water	1500	0	...	...	1.0
Silt/sand	1600	0.2	400	0.5	1.6
Sand	1800	0.1	600	0.2	1.8
Granite	5000	0.01	2500	0.02	2.4

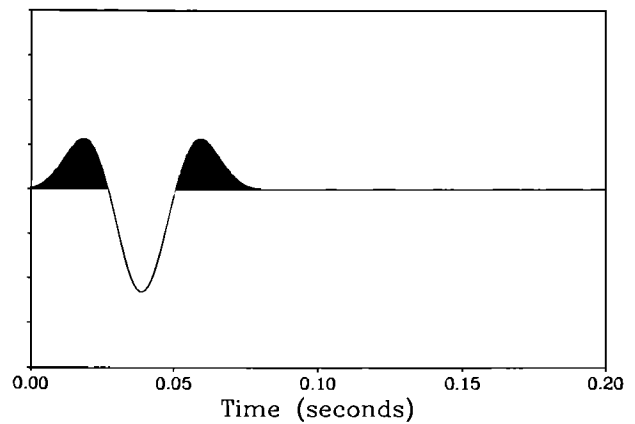


FIG. 9. Second-order Blackman-Harris source pulse with center frequency 20 Hz.

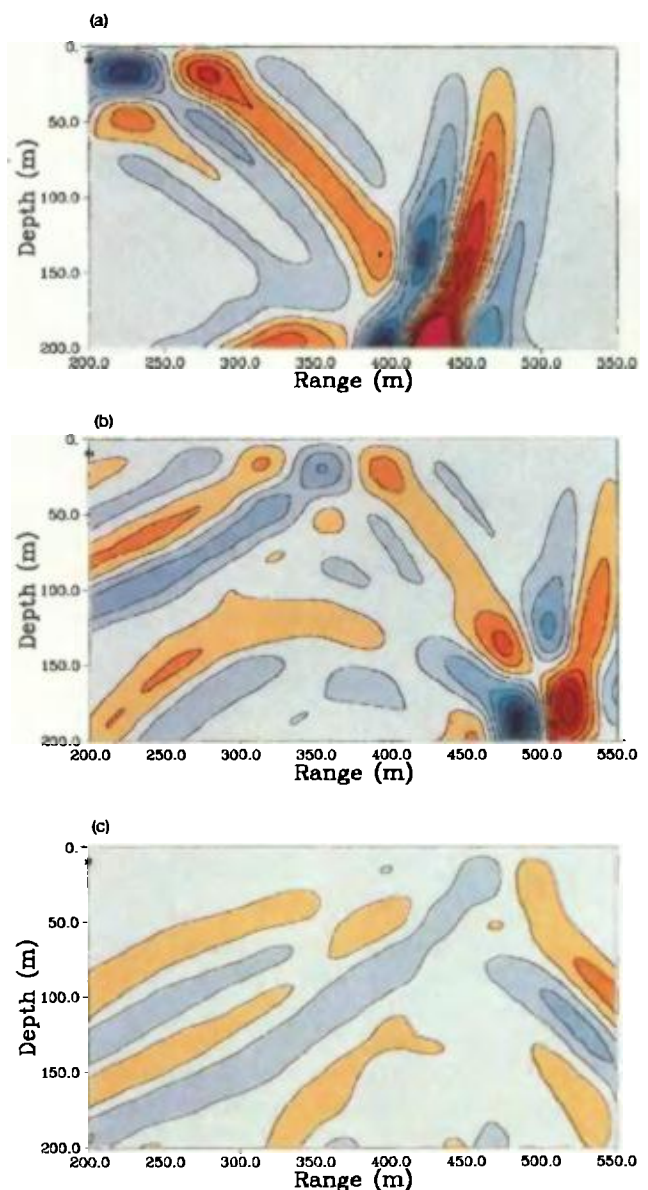


FIG. 10. Snapshot contours of full acoustic field at times (a) 0.35 s, (b) 0.40 s, and (c) 0.45 s. Positive stress (negative pressure) amplitude indicated by red colors, negative by blue colors.

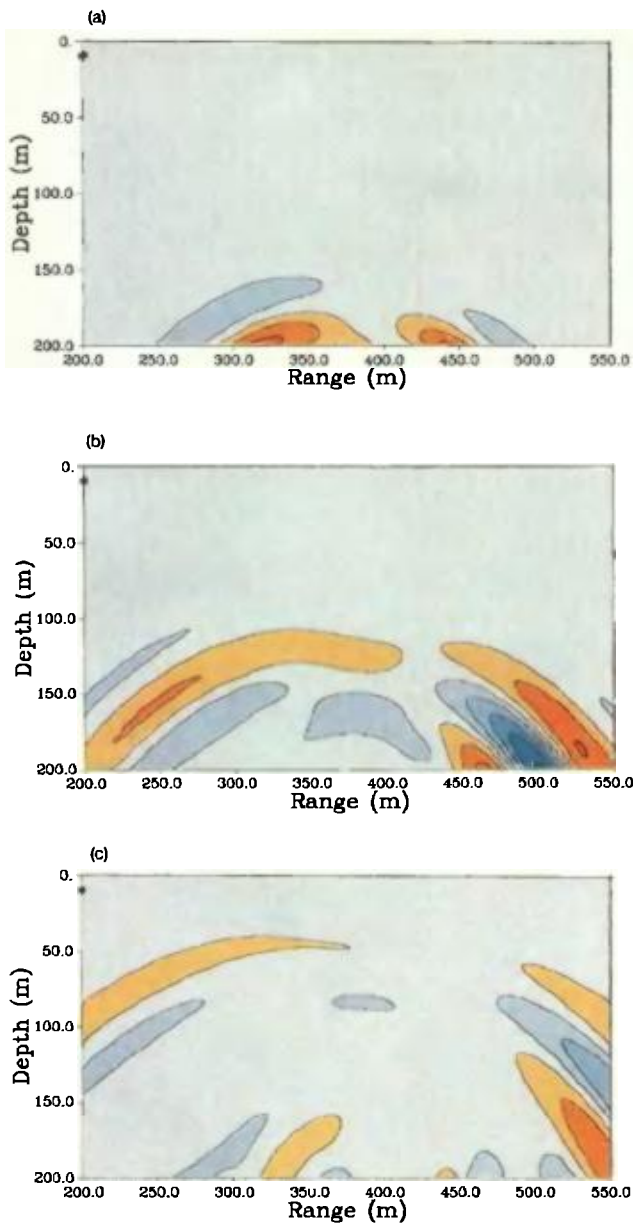


FIG. 11. Snapshot contours of scattered acoustic field at times (a) 0.35 s, (b) 0.40 s, and (c) 0.45 s. Positive stress (negative pressure) amplitude indicated by red colors, negative by blue colors.

but the temporal structure of the scattered field is much more easily interpreted by eliminating the physical source field, as done in Fig. 12 (b).

Figure 13 shows the stacked time series for a geophone array placed on the seabed at depth 200 m, ranging from 200- to 550-m range, i.e., covering both the forward and back-scattering regions. Figure 13(a) and (b) shows the vertical geophone component for the total field and scattered field, respectively, and 13(c) shows the corresponding horizontal geophone components. Multiple scattering from the inclusion is evident, with the earliest arrival appearing at slightly shorter range than the center of the facet, consistent with the

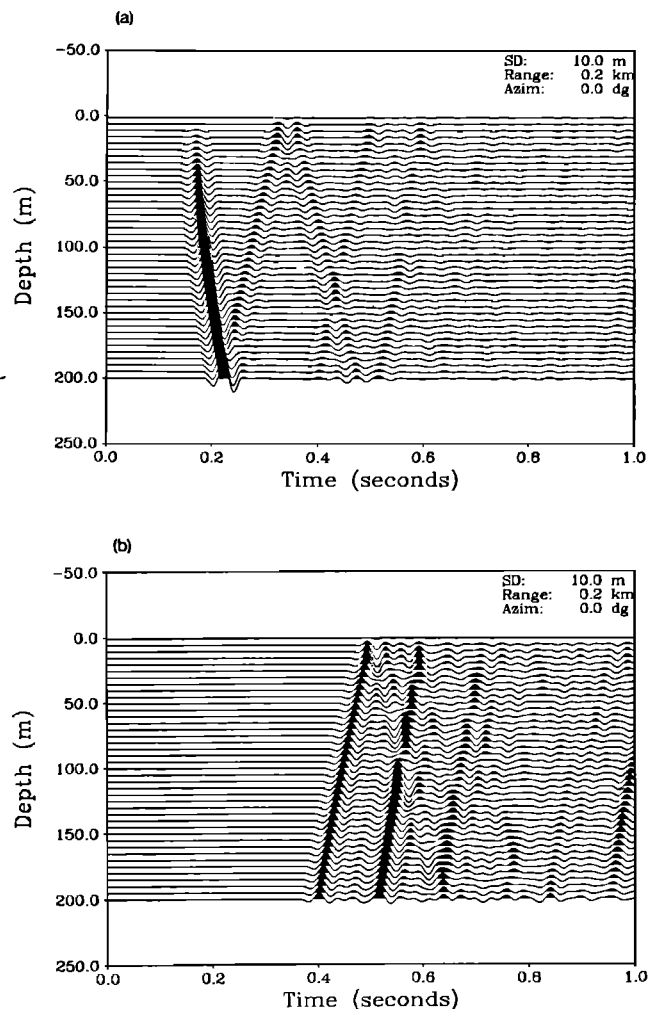


FIG. 12. Stacked time series on vertical hydrophone array spanning whole water column at range 200 m from source, 200 m from inclusion in the backward direction. (a) Full field; (b) scattered field.

snapshots of the scattered field in Fig. 11. It is interesting to note that the converted shear and Scholte waves are dominating the scattered field.

We chose a circular inclusion for simplicity, but the method and the code do not make any assumption regarding symmetry and an arbitrary shape could have been chosen. For the actual modeling of the inclusion, 40 elements were used.

In order to find the time response from 0–1 s, we computed the response at frequencies in the range from 0–46 Hz. The influence matrix for both the exterior and interior was computed using the same wave number sampling parameters as in the previous examples. For computation of the source contribution at the scatterer and for propagation of the solution from the scatterer, the wave number response was sampled at 1024 points in the horizontal phase velocity interval from  $-200$  to  $200$  m/s. The total computation time for this example was 2.5 h on an Alliant FX-40 with two processors and 10 min on a Cray-2.

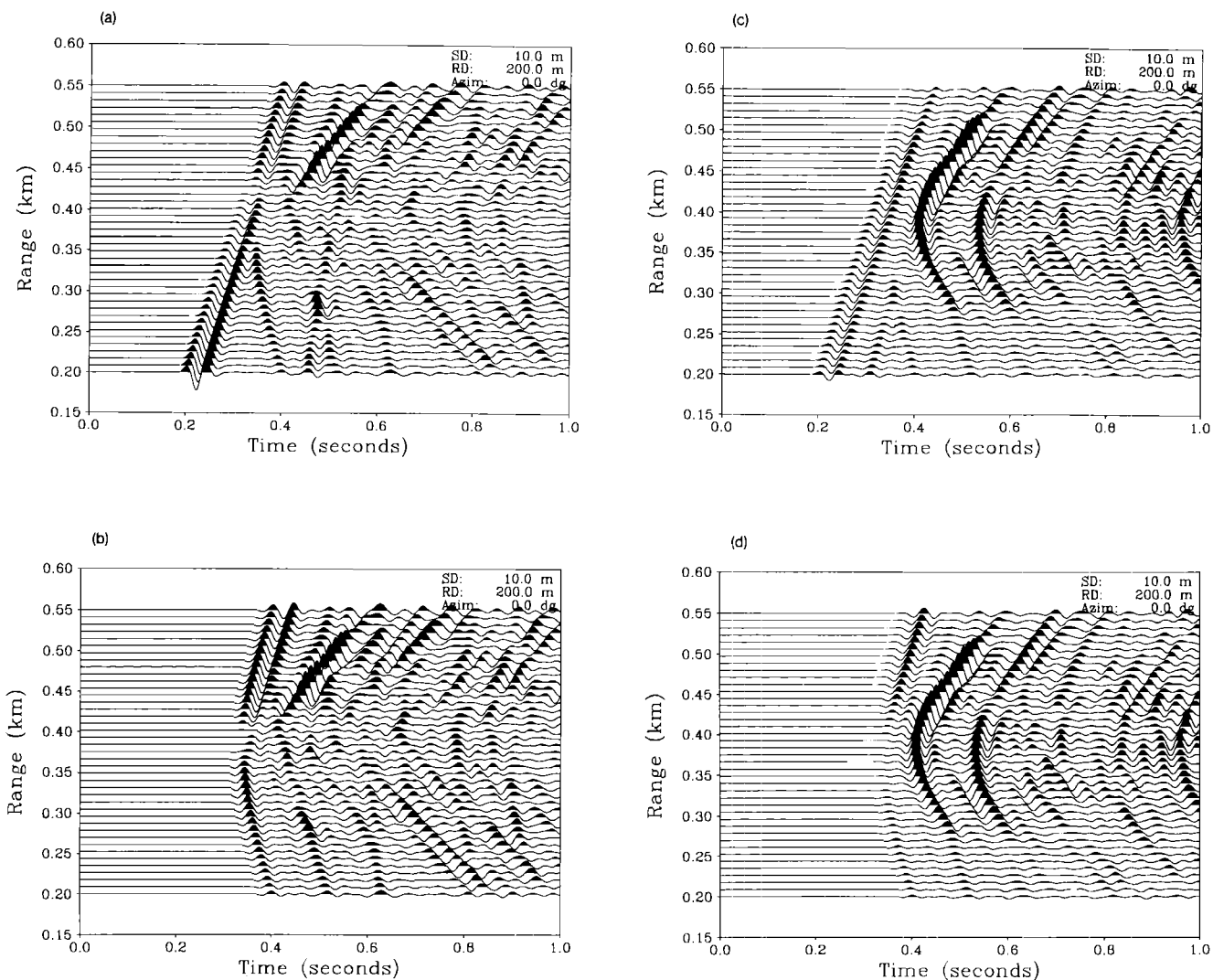


FIG. 13. Stacked, synthetic time series for geophones on the seabed 200- to 550-m range from source, above facet. (a) Vertical velocity, total field; (b) vertical velocity, scattered field; (c) horizontal velocity, total field; and (d) horizontal velocity, scattered field.

## V. CONCLUSIONS

A hybrid boundary element-wave number integration approach has been presented for simulation of two-dimensional seismoacoustic scattering and reverberation from facets in an arctic ice cover and a stratified elastic seabed. There are several advantages of the present hybrid BEM-WI approach compared to the alternative discrete methods:

(1) The discretization is limited to the boundary of the facet.

(2) Short- as well as long-range reverberation can be treated efficiently.

(3) In terms of basic understanding of the factors affecting ocean seismoacoustic reverberation, an important advantage of the present approach is its inherent spectral decomposition of the total solution in both the frequency and wave number domains.

(4) The reverberated field can be directly separated from the total field, significantly aiding the interpretation.

(5) The DGM-BEM approach is extendable to three dimensions due to the fact that only the facet boundary needs to be discretized.

The present DGM-BEM is of more general applicability to ocean seismoacoustic reverberation problems than earlier published hybrid boundary integral-wavenumber integration methods due to the following inherent features:

(1) Both exterior and interior domains can be stratified fluid-elastic media, including transversely isotropic layers.

(2) Efficient computation of the Green's functions for stratified exterior and interior domains by means of modified DGM-SAFARI code.

(3) Closed form element integrations significantly increase the accuracy and thus reduce the discretization requirements.

(4) Reverberant field computed by the existing seismoacoustic propagation model, retaining all existing features in terms of environmental models and outputs available.

## ACKNOWLEDGMENTS

The work was supported in part the Danish Technology Council and the Office of Naval Research (Arctic Program and Structural Acoustics Program Offices). Some calculations described in this paper were performed on the MIT Supercomputer Facility CRAY-2.

- <sup>1</sup> A. B. Baggeroer, W. A. Kuperman, and H. Schmidt, "Matched field processing: source localization in correlated noise as an optimum parameter estimation problem," *J. Acoust. Soc. Am.*, **83**, 571–587 (1988).
- <sup>2</sup> W. A. Kuperman and F. Ingenito, "Spatial correlation of surface generated noise in a stratified ocean," *J. Acoust. Soc. Am.*, **67**, 1988–1996 (1980).
- <sup>3</sup> E. I. Thorsos and D. R. Jackson, "The validity of the perturbation approximation for rough surface scattering using a Gaussian roughness spectrum," *J. Acoust. Soc. Am.*, **86**, 261–277 (1989).
- <sup>4</sup> D. K. Dacol and D. H. Berman, "Sound scattering from a randomly rough fluid–solid interface," *J. Acoust. Soc. Am.*, **84**, 292–302 (1988).
- <sup>5</sup> W. A. Kuperman and H. Schmidt, "Self-consistent perturbation approach to rough surface scattering in stratified elastic media," *J. Acoust. Soc. Am.*, **86**, 1511–1522 (1989).
- <sup>6</sup> J. A. Ogilvy, "Wave scattering from rough surfaces," *Rep. Prog. Phys.* **50**, 1553–1608 (1987).
- <sup>7</sup> R. B. Evans, "A coupled mode solution for propagation in a waveguide with stepwise depth variations of a penetrable bottom," *J. Acoust. Soc. Am.*, **74**, 188–195 (1983).
- <sup>8</sup> M. E. Dougherty and R. A. Stephen, "Geoacoustic scattering from sea-floor features in ROSE area," *J. Acoust. Soc. Am.*, **82**, 238–256 (1987).
- <sup>9</sup> J. R. Fricke, R. A. Stephen, and A. B. Baggeroer, "Numerical modeling of the scattered acoustic field from elastic ice," *J. Acoust. Soc. Am. Suppl.* **1** **83**, S37 (1988).
- <sup>10</sup> B. L. N. Kennett, "Reflections, rays and reverberations," *Bull. Seismol. Soc. Am.*, **71**, 1011–1029 (1974).
- <sup>11</sup> M. Bouchon and K. Aki, "Discrete wavenumber representation of seismic source wavefields," *Bull. Seismol. Soc. Am.*, **67**, 259–277 (1977).
- <sup>12</sup> H. Schmidt and G. Tango, "Efficient global matrix approach to the computation of synthetic seismograms," *Geophys. J. R. Astron. Soc.* **84**, 331–359 (1986).
- <sup>13</sup> M. B. Porter, "The time-marched fast-field program (FFP) for modeling acoustic pulse propagation," *J. Acoust. Soc. Am.*, **87**, 2013–2023 (1990).
- <sup>14</sup> F. Ingenito, "Scattering from an object in a stratified medium," *J. Acoust. Soc. Am.*, **82**, 2051–2059 (1987).
- <sup>15</sup> R. H. Hackman and G. S. Sammelmann, "Multiple-scattering analysis for a target in an oceanic waveguide," *J. Acoust. Soc. Am.*, **84**, 1813–1825 (1988).
- <sup>16</sup> G. T. Schuster and L. C. Smith, "Modeling scatterers embedded in a plane-layered media by a hybrid Haskell–Thomson and boundary integral equation method," *J. Acoust. Soc. Am.*, **78**, 1387–1394 (1985).
- <sup>17</sup> T. W. Dawson and J. A. Fawcett, "A boundary integral equation method for acoustic scattering in a waveguide with nonplanar surfaces," *J. Acoust. Soc. Am.*, **87**, 1110–1125 (1990).
- <sup>18</sup> M. A. Bravo, F. J. Sánchez-sesma, and F. J. Chávez Garcia, "Ground motion on stratified alluvial deposits for incident *SH* waves," *Bull. Seismol. Soc. Am.*, **78**, 436–450 (1988).
- <sup>19</sup> M. Campillo, "Modelling of *SH* wave propagation in an irregularly layered medium—Application to seismic profiles near a dome," *Geophys. Prospect.* **35**, 236–249 (1987).
- <sup>20</sup> M. Bouchon, "A simple, complete numerical solution to the problem of diffraction of *SH* waves by an irregular surface," *J. Acoust. Soc. Am.*, **77**, 1–5 (1985).
- <sup>21</sup> H. Kawase, "Time-domain response of a semi-circular canyon for incident *SV*, *P* and Rayleigh waves calculated by the discrete wavenumber boundary element method," *Bull. Seismol. Soc. Am.*, **78**, 1415–1437 (1988).
- <sup>22</sup> H. Kawase and K. Aki, "A study on the response of a soft basin for incident *S*, *P* and Rayleigh waves with special reference to the long duration observed in Mexico City," *Bull. Seismol. Soc. Am.*, **79**, 1361–1482 (1989).
- <sup>23</sup> H. Kawase and K. Aki, "Topography effect at the critical *SV* wave incidence: Possible explanations of damage pattern by the Whittier Narrows, California earthquake of 1 October 1987," *Bull. Seismol. Soc. Am.*, **80**, 1–22 (1990).
- <sup>24</sup> H. Schmidt and F. B. Jensen, "A full wave solution for propagation in multilayered viscoelastic media with application to Gaussian beam reflection at fluid–solid interfaces," *J. Acoust. Soc. Am.*, **77**, 813–825 (1985).
- <sup>25</sup> W. M. Ewing, W. S. Jardetzky, and F. Press, *Elastic Waves in Layered Media* (McGraw-Hill, New York, 1957).
- <sup>26</sup> J. Miklowitz, *The Theory of Elastic Waves and Waveguides* (North-Holland, New York, 1984).
- <sup>27</sup> W. T. Thomson, "Transmission of elastic waves through a stratified solid," *J. Appl. Phys.* **21**, 89–93 (1950).
- <sup>28</sup> N. A. Haskell, "The dispersion of surface waves in multilayered media," *Bull. Seismol. Soc. Am.*, **43**, 17–34 (1953).
- <sup>29</sup> H. Schmidt, "SAFARI: Seismo-acoustic fast field algorithm for range independent environments. User's Guide," SR 113, SACLANT ASW Research Centre, La Spezia, Italy (1987).
- <sup>30</sup> J. S. Kim, "Radiation from directional seismic sources in laterally stratified media with application to Arctic ice cracking noise," Ph.D. thesis, Massachusetts Institute of Technology (May 1989).
- <sup>31</sup> I. S. Gradshteyn and I. M. Ryzhik, *Table of Integrals, Series and Products* (Academic, New York, 1980).
- <sup>32</sup> A. T. deHoop, "Reciprocity theorems for acoustic wave fields in fluid/solid configuration," *J. Acoust. Soc. Am.*, **87**, 1932–1937 (1990).
- <sup>33</sup> H. L. Wong, "Effect of surface topology on the diffraction of *P*-, *SV* and Rayleigh waves," *Bull. Seismol. Soc. Am.*, **72**, 1167–1183 (1982).
- <sup>34</sup> S. Krenk, P. Gerstoft, and O. Vilmann, "Computational aspects of synthetic seismograms for layered media," In *Proceedings of the 59th SEG Meeting*, Dallas, (Publisher, City, 1989), pp. 1086–1089.
- <sup>35</sup> O. Vilmann, P. Gerstoft, and S. Krenk, "High-speed forward modelling in seismic data processing," Tech. Rep., Ødegard and Danneskiold-Samsøe (1989).